1-1-2013

Tunable terahertz emission from the intrinsic Josephson junctions in acute isosceles triangular Bi2Sr2CaCu2O8+delta mesas

K. Delfanazari

H. Asai

M. Tsujimoto

T. Kashiwagi

T. Kitamura

Tunable terahertz emission from the intrinsic Josephson junctions in acute isosceles triangular $Bi_2Sr_2CaCu_2O_{8+\delta}$ mesas

K. Delfanazari,[1,2,3,*] H. Asai,[4] M. Tsujimoto,[1,2,3] T. Kashiwagi,[1,2,3] T. Kitamura,[1,2,3] T. Yamamoto,[5] M. Sawamura,[1,2,3] K. Ishida,[1,2,3] C. Watanabe,[1,2,3] S. Sekimoto,[1,2,3] H. Minami,[1,2,3] M. Tachiki,[1,2] R. A. Klemm,[6] T. Hattori,[1,2] and K. Kadowaki,[1,2,3,7]

[1]*Graduate School of Pure and Applied Sciences, University of Tsukuba, Tsukuba 305-8573, Japan*
[2]*CREST-JST, Kawaguchi Center Building, 4-1-8 Hon-cho, Kawaguchi 332-0012, Japan*
[3]*WPI-MANA, International Center for Materials Nanoarchitectonics, 1-1 Namiki, Tsukuba 305-0044, Japan*
[4]*Electronics and Photonics Research Institute, The National Institute of Advanced Industrial Science and Technology (AIST), Tsukuba, Ibaraki 305-8568, Japan*
[5]*Semiconductor Analysis and Radiation Effects Group, Japan Atomic Energy Agency, Gunma 370-1292, Japan*
[6]*Department of Physics, University of Central Florida, Orlando, Florida 32816, USA*
[7]*kadowaki@ims.tsukuba.ac.jp*
[*]*s-kaveh@ims.tsukuba.ac.jp*

Abstract: In order to determine if the mesa geometry might affect the properties of the coherent terahertz (THz) radiation emitted from the intrinsic Josephson junctions in mesas constructed from single crystals of the high-temperature superconductor, $Bi_2Sr_2CaCu_2O_{8+\delta}$, we studied triangular mesas. For equilateral triangular mesas, the observed emission was found to be limited to the single mesa TM(1,0) mode. However, tunable radiation over the range from 0.495 to 0.934 THz was found to arise from an acute isosceles triangular mesa. This 47% tunability is the widest yet observed from the outer current-voltage characteristic branch of such mesas of any geometry. Although the radiation at a few of the frequencies in the tunable range appear to have been enhanced by cavity resonances, most frequencies are far from such resonance frequencies, and can only be attributed to the ac-Josephson effect.

OCIS codes: (190.4720) Optical nonlinearities of condensed matter; (270.1670) Coherent optical effects.

References and links

1. M. Tonouchi, "Cutting-edge terahertz technology," Nat. Photonics **1**(2), 97–105 (2007).
2. B. D. Josephson, "Possible new effects in superconductive tunneling," Phys. Rev. Lett. **1**, 251–253 (1962).
3. D. N. Langenberg, D. J. Scalapino, B. N. Taylor, and R. E. Eck, "Investigation of microwave radiation emitted by Josephson junctions," Phys. Rev. Lett. **15**(7), 294–297 (1965).
4. I. K. Yanson, V. M. Svistunov, and I. M. Dmitrenko, "Experimental observation of tunned effect for Cooper pairs with emission of photons," Sov. Phys. JETP **21**, 650–652 (1965).
5. P. Barbara, A. B. Cawthorne, S. V. Shitov, and C. J. Lobb, "Stimulated emission and amplification in Josephson junction arrays," Phys. Rev. Lett. **82**(9), 1963–1966 (1999).
6. R. Kleiner, F. Steinmeyer, G. Kunkel, and P. Müller, "Intrinsic Josephson effects in $Bi_2Sr_2CaCu_2O_{8+\delta}$ single crystals," Phys. Rev. Lett. **68**(15), 2394–2397 (1992).
7. L. Ozyuzer, A. E. Koshelev, C. Kurter, N. Gopalsami, Q. Li, M. Tachiki, K. Kadowaki, T. Yamamoto, H. Minami, H. Yamaguchi, T. Tachiki, K. E. Gray, W.-K. Kwok, and U. Welp, "Emission of coherent THz radiation from superconductors," Science **318**(5854), 1291–1293 (2007).
8. K. Kadowaki, H. Yamaguchi, K. Kawamata, T. Yamamoto, H. Minami, I. Kakeya, U. Welp, L. Ozyuzer, A. Koshelev, C. Kurter, K. E. Gray, and W.-K. Kwok, "Direct observation of terahertz electromagnetic waves emitted from intrinsic Josephson junctions in single crystalline $Bi_2Sr_2CaCu_2O_{8+\delta}$," Physica C **468**(7–10), 634–639 (2008).
9. M. Tsujimoto, T. Yamamoto, K. Delfanazari, R. Nakayama, T. Kitamura, M. Sawamura, T. Kashiwagi, H. Minami, M. Tachiki, K. Kadowaki, and R. A. Klemm, "Broadly Tunable Subterahertz Emission from Internal Branches of the Current-Voltage Characteristics of Superconducting $Bi_2Sr_2CaCu_2O_{8+\delta}$ Single Crystals," Phys. Rev. Lett. **108**, 107006 (2012).

#179100 - $15.00 USD Received 5 Nov 2012; revised 28 Dec 2012; accepted 29 Dec 2012; published 22 Jan 2013

10. K. Yamaki, M. Tsujimoto, T. Yamamoto, A. Furukawa, T. Kashiwagi, H. Minami, and K. Kadowaki, "High-power terahertz electromagnetic wave emission from high-T_c superconducting mesa structures," Opt. Express **19**, 3193–3201 (2011).
11. K. Kadowaki, M. Tsujimoto, K. Yamaki, T. Yamamoto, T. Kashiwagi, H. Minami, M. Tachiki, and R. A. Klemm, "Evidence for a dual-source mechanism of THz radiation from rectangular mesas of single crystalline $Bi_2Sr_2CaCu_2O_{8+\delta}$ intrinsic Josephson junctions," J. Phys. Soc. Jpn. **79**(2), 023703 (2010).
12. H. Minami, I. Kakeya, H. Yamaguchi, T. Yamamoto, and K. Kadowaki, "Characteristics of terahertz radiation emitted from the intrinsic Josephson junctions in high-T_c superconductor $Bi_2Sr_2CaCu_2O_{8+\delta}$," Appl. Phys. Lett. **95**(23), 232511 (2009).
13. H. B. Wang, S. Guénon, J. Yuan, A. Iishi, S. Arisawa, T. Hatano, T. Yamashita, D. Koelle, and R. Kleiner, "Hot spots and waves in $Bi_2Sr_2CaCu_2O_8$ intrinsic Josephson junction stacks: a study by low temperature scanning laser microscopy," Phys. Rev. Lett. **102**(1), 017006 (2009).
14. H. B. Wang, S. Guénon, B. Gross, J. Yuan, Z. G. Jiang, Y. Y. Zhong, M. Grünzweig, A. Iishi, P. H. Wu, T. Hatano, D. Koelle, and R. Kleiner, "Coherent terahertz emission of intrinsic Josephson junction stacks in the hot spot regime [corrected]," Phys. Rev. Lett. **105**(5), 057002 (2010).
15. H. Minami, N. Orita, T. Koike, T. Yamamoto, and K. Kadowaki, "Continuous and reversible operation of Bi2212 based THz emitters just below T_c," Physica C **470**, S822–S823 (2010).
16. T. Kashiwagi, M. Tsujimoto, T. Yamamoto, H. Minami, K. Yamaki, K. Delfanazari, K. Deguchi, N. Orita, T. Koike, R. Nakayama, T. Kitamura, M. Sawamura, S. Hagino, K. Ishida, K. Ivanovic, H. Asai, M. Tachiki, R.A. Klemm, and K. Kadowaki, "High temperature superconductor THz emitters: Fundamental physics and its applications," Jpn. J. Appl. Phys. **51,** 010113 (2012).
17. T. Kashiwagi, K. Yamaki, M. Tsujimoto, K. Deguchi, N. Orita, T. Koike, R. Nakayama, H. Minami, T. Yamamoto, R.A. Klemm, M. Tachiki, and K. Kadowaki, "Geometrical Full-wavelength resonance mode generating terahertz waves from a single crystalline $Bi_2Sr_2CaCu_2O_{8+\delta}$ rectangular mesa," J. Phys. Soc. Jpn. **80**, 094709 (2011).
18. R. A Klemm and K. Kadowaki, "Output from a Josephson stimulated terahertz amplified radiation emitter," J. Phys.: Condens. Matter **22**, 375701 (2010).
19. R. A. Klemm and K. Kadowaki, "Angular dependence of the radiation power of a Josephson STAR-emitter," J. Supercond. Novel Magn. **23**(5), 613–616 (2010).
20. M. Tsujimoto, K. Yamaki, K. Deguchi, T. Yamamoto, T. Kashiwagi, H. Minami, M. Tachiki, K. Kadowaki, and R. A. Klemm, "Geometrical resonance conditions for THz radiation from the intrinsic Josephson junctions in $Bi_2Sr_2CaCu_2O_{8+\delta}$," Phys. Rev. Lett. **105**(3), 037005 (2010).
21. S. Guénon, M. Grünzweig, B. Gross, J. Yuan, Z. G. Jiang, Y. Y. Zhong, A. Iishi, P. H. Wu, T. Hatano, D. Koelle, H. B. Wang, and R. Kleiner, "Interaction of hot spots and THz waves in $Bi_2Sr_2CaCu_2O_8$ intrinsic Josephson junction stacks of various geometry," Phys. Rev. B **82**(21), 214506 (2010).
22. T. M. Benseman, A. E. Koshelev, K. E. Gray, W.-K. Kwok, U. Welp, K. Kadowaki, M. Tachiki, and T. Yamamoto, "Tunable terahertz emission from $Bi_2Sr_2CaCu_2O_{8+\delta}$ mesa devices," Phys. Rev. B **84**(6), 064523 (2011).
23. M. Li, J. Yuan, N. Kinev, J. Li, B. Gross, S. Guénon, A. Ishii, K. Hirata, T. Hatano, D. Koelle, R. Kleiner, V. P. Koshelets, H. Wang, and P. Wu, "Linewidth dependence of coherent terahertz emission from $Bi_2Sr_2CaCu_2O_{8+\delta}$ intrinsic Josephson junction stacks in the hot-spot regime," Phys. Rev. B **86**(6), 060505 (2012).
24. N. Orita, H. Minami, T. Koike, T. Yamamoto, and K. Kadowaki, "Synchronized operation of two serially connected Bi2212 THz emitters," Physica C **470**, S786–S787 (2010).
25. I. J. Bahl and P. Bhartiya, *Microstrip Antennas* (Artech House, 1980).
26. K. Arvind Sharma and B. Bhat, "Analysis of triangular microstrip resonators," IEEE, Trans. Microwave Theory Technol. **30**, 2029–2031 (1982).
27. P. L. Overfelt and D. J. White, "TE and TM modes of some triangular cross-section waveguides using superposition of plane waves," IEEE, Trans. Microwave Theory Technol. **34**(1), 161–167 (1986).
28. T. Mochiku and K. Kadowaki, "Growth and properties of Bi_2Sr_2 (Ca,Y)$Cu_2O_{8+\delta}$ single crystals," Physica C, 235–240, 523 (1994).
29. K. Delfanazari, H. Asai, M. Tsujimoto, T. Kashiwagi, T. Kitamura, T. Yamamoto, M. Sawamura, K. Ishida, M. Tachiki, R. A. Klemm, T. Hattori, and K. Kadowaki, "Study of the coherent and continuous terahertz wave emission in equilateral triangular mesas of superconducting $Bi_2Sr_2CaCu_2O_{8+\delta}$ intrinsic Josephson junctions," Physica C (in press, doi.org/10.1016/j.physc.2012. 12.009).
30. R. A. Klemm, K. Delfanazari, M. Tsujimoto, T. Kashiwagi, T. Kitamura, T. Yamamoto, M. Sawamura, K. Ishida, T. Hattori, and K. Kadowaki, "Modeling the electromagnetic cavity mode contributions to the THz emission from triangular $Bi_2Sr_2CaCu_2O_{8+\delta}$ mesas," Physica C (in press, doi.org/10.1016/j.physc.2012. 11.006).
31. K. Delfanazari, M. Tsujimoto, T. Kashiwagi, T. Yamamoto, R. Nakayama, S. Hagino, T. Kitamura, M. Sawamura, T. Hattori, H. Minami, and K. Kadowaki, "THz emission from a triangular mesa structure of Bi-2212 intrinsic Josephson junctions," J. Phys.: Conf. Ser. **400**(2), 022014 (2012).
32. H. Asai, M. Tachiki, and K. Kadowaki, "Three-dimensional numerical analysis of terahertz radiation emitted from intrinsic Josephson junctions with hot spots," Phys. Rev. B **85**(6), 064521 (2012).
33. A. E. Koshelev and L. N. Bulaevskii, "Resonant electromagnetic emission from intrinsic Josephson-junction states with laterally modulated Josephson critical current," Phys. Rev. B **77**(1), 014530 (2008).
34. V. M. Krasnov, "In-plane fluxon in layered superconductors with arbitrary number of layers," Phys. Rev. B **63**(6), 064519 (2001).
35. S. O. Katterwe and V. M. Krasnov, "Temperature dependence of geometrical and velocity-matching resonances in $Bi_2Sr_2CaCu_2O_{8+x}$ intrinsic Josephson junctions," Phys. Rev. B **84**(21), 214519 (2011).

#179100 - $15.00 USD Received 5 Nov 2012; revised 28 Dec 2012; accepted 29 Dec 2012; published 22 Jan 2013

1. Introduction

The frequencies of terahertz (THz) electromagnetic (EM) waves lie between those of microwaves and infrared radiation. This frequency range encompasses the vibrational frequencies of various kinds of molecules and materials. Moreover, in recent years, the application of THz technology has become a key issue for research in ultra-high speed communications, quantum information, pharmaceutical industries, medicine and medical diagnoses, bio-sciences and biotechnologies, non-destructive sensing and testing, and various kinds of imaging purposes, *etc* [1]. At present, small-scale electron tube devices [backward wave oscillators], solid state devices such as quantum cascade lasers (QCLs), resonant tunneling diodes, and uni-traveling carrier photodiodes, *etc.*, are available techniques for generating THz waves. However, they are mostly large, cumbersome devices with accessory components. A compact source which can generate intense THz EM waves is thus highly desirable.

The ac-Josephson effect intrinsic to an atomic-scale layered superconductor can provide such a source. Application of a dc voltage V across a single Josephson junction between identical superconductors leads to an ac-Josephson current and EM radiation at the frequency f that satisfies the ac-Josephson relation, $f = f_J = (2e/h)V$, where e is the electronic charge and h is Planck's constant [2–4]. Using two-dimensional arrays of Josephson junctions between wires of superconducting Nb, coherent radiation was observed when the array was placed parallel to a Nb ground plane [5], that amplified the radiation, but did not affect its frequency, which obeyed the Josephson relation. However, the technical problems involved in mass productions were formidable.

The layered high transition temperature (T_c) superconductor $Bi_2Sr_2CaCu_2O_{8+\delta}$ (Bi-2212), behaves as a stack of intrinsic Josephson junctions (IJJs) [6]. In Bi-2212, each of the junctions is naturally identical, as they are evenly spaced with two junctions per unit cell c-axis edge length of 1.533 nm. Recently, coherent continuous-wave THz radiation was induced by applying a V across the stack of N IJJs present in small mesas milled out of single crystalline Bi-2212 [7]. The coherence was established by examining the radiation in the retrapping region in the lower part of the current-voltage characteristics (IVCs), in which the number N changes as V jumps discontinuously, but the power was found to behave as N^2 [7]. Hence, the output power for N~10^3 junctions in a mesa is roughly 10^6 times larger than that observed from a single Josephson junction, bringing the output power into the μW range [7–17].

Most measurements of THz wave generation from Bi-2212 were made using rectangular mesas [7–23], although disk and square mesas were also studied [18–21]. Since Bi-2212 is extremely anisotropic, behaving for $\boldsymbol{E} \parallel \hat{\boldsymbol{c}}$ as an insulator [6], the three-dimensional mesa structure also behaves as an internal EM cavity, which usually couples to the non-linear ac-Josephson currents generated in each IJJ [7–21]. Therefore, the characteristic radiation has been understood to arise primarily from the electric dipole radiation due to the uniform part of the ac-Josephson current along the c-axis satisfying $f = f_J$, which can sometimes also be enhanced by the excitation of an internal mesa cavity resonance at the mode frequency f_{mn}^c determined by the mesa shape, by the ac-Josephson current's non-uniform part [18–20]. Strong coupling (or excitation) to the internal cavity results in sharp resonant emission at one or more transverse magnetic cavity mode frequencies, but weak coupling gives rise to broadband emission tunable over a wide frequency range [9,14]. This tunability has so far been enhanced by two procedures: by producing groove mesas using focused ion beam (FIB) milling, which may modify the boundary conditions, and by examining the radiation emitted from the inner IVC branches [9]. In all cases studied to date, the emission frequency still obeys the ac-Josephson relation $f = f_J = (2e/h)V/N$, for N radiating junctions, so that V/N is the voltage across each IJJ in the stack [9].

#179100 - $15.00 USD Received 5 Nov 2012; revised 28 Dec 2012; accepted 29 Dec 2012; published 22 Jan 2013

One issue of current study is the nature of the synchronization of the radiation emitted from the different IJJs. The intrinsic radiation linewidths can be extremely narrow, and are usually much less than the resolution of the Fourier transform infrared (FT-IR) spectrometer of 7-12 GHz, depending upon the equipment used. Frequency mixing experiments determined the linewidth to be 500 MHz [16]. Another experiment suggested that at high I bias, the intrinsic linewidth may be as low as 23 MHz [23]. Several models have been proposed, but there is no consensus as to why such narrow linewidths could arise, especially with strongly spatially inhomogeneous heating effects present during emission [23].

There have been efforts at enhancing the emission power by the synchronization of arrays of radiating rectangular mesas obtained from the same crystal [24]. Such experiments have confirmed the locking of the radiation from different adjacent mesas onto one f value, with the associated increase in output power characteristic of overall coherence. Triangular geometries are promising candidates for synchronization purposes because of their circular polarization features important in array design [25]. Additionally, triangular shapes are also interesting to study because for an acute isosceles triangular mesa, the resonant frequencies are inversely proportional to the length (the distance from the apex of the triangle to its base) of the mesa and almost independent of its basal width [25–27], so that variation of the mesa shapes can be useful in producing enhanced tunability.

In this study, we present tunable, coherent, and continuous-wave THz emission from acute isosceles triangular mesas fabricated by FIB milling of single crystalline Bi-2212. We studied experimentally the IVCs and the emission spectra using a Fourier transform infrared spectrometer, in order to elucidate the radiation mechanism of the triangular mesa samples. We found that the emission frequencies were nearly continuous from 0.495 to 0.934 THz. This 47% tunability is the largest tunability range yet reported from the outer IVC branch of any Bi-2212 mesa [9,14,22]. In all cases, the radiation frequency $f = f_J$ satisfies the ac-Josephson relation described above. For comparison, we also studied equilateral triangular mesas. For each of the equilateral triangular mesas, THz radiation was only observed when f was in the vicinity of a known cavity resonant frequency determined by the mesa geometry.

The nearly continuous wide spectrum emitted from an acute isosceles triangle also exhibits a large peak at 0.61 THz, and a few other smaller peaks. Since the analytical cavity modes of isosceles triangular resonators were not previously known, we numerically investigated the internal EM cavity modes of the IJJ mesas using the finite difference time domain (FDTD) method, and solved for the exact cavity modes of a pie-shaped wedge mesa closely approximating the acute isosceles triangular mesa shapes under study. Both calculations predict the largest peak in the observed frequency spectrum of an acute isosceles triangular mesa, and the simple pie-shaped wedge model also predicts some other weaker peaks in the frequency spectrum. However, there remain wide regions of the continuous spectrum that are not associated with any wedge cavity mode frequency, so that the tunable spectrum is mostly free of cavity effects.

2. Sample preparation and methods

A large Bi-2212 single crystal was grown by the travelling solvent floating zone technique inside a special ellipsoid-shaped Au-coated chamber [28]. A piece of the crystal with lateral sizes of 10 × 5 mm^2 was annealed at 650 °C for 24 hours in argon gas mixed with 0.1% of oxygen to produce slightly underdoped crystals, which are essential for producing coherent emission. A smaller piece of this crystal with lateral sizes of 800 × 800 μm^2 was glued onto a sapphire substrate using silver paste. We then cleaved the crystal with Scotch tape in order to obtain a clean surface, upon which thin layers of Ag and Au were evaporated. Equilateral and isosceles triangular mesas were fabricated by FIB, and Au electrical lead wires 10 μm in diameter were attached by Ag paste, as schematically shown in Fig. 1(a). Note that the mesa (inside the groove), the substrate (below the mesa), and the surrounding material (outside the groove) are all part of the same Au-coated single crystal of Bi-2212. Two combined scanning ion microscopy (SIM) micrographs of two triangular samples are shown in Fig. 1(b).

#179100 - $15.00 USD Received 5 Nov 2012; revised 28 Dec 2012; accepted 29 Dec 2012; published 22 Jan 2013

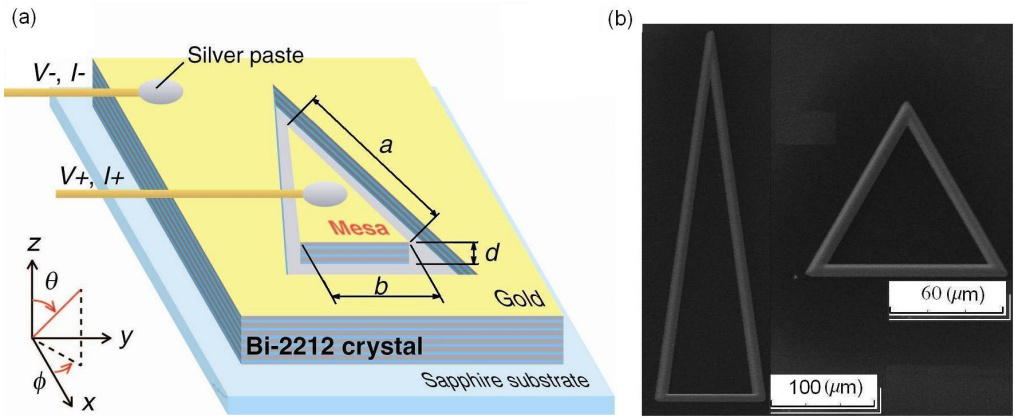

Fig. 1. (a) A schematic view of an acute isosceles triangular mesa. Thin layers of Ag and Au are coated on the surface of the single crystal. Two gold wires are attached on both sides of the groove etched into the single crystal in order to apply current in the *c*-axis direction of Bi-2212. (b) Two combined scanning ion microscopy images of an isosceles and an equilateral triangular mesa.

The dimensions of the mesas (see Table 1) were measured by an atomic force microscope, resulting in clear trapezoidal cross-sectional mesa shapes, in which the bottom lengths of the mesa (presented in Table 1) are about 3-5 μm larger than the top lengths (not presented). The sample transition temperatures and their widths were measured from the *c*-axis resistivities, as shown for one sample in Fig. 2(a).

The mesas were biased using a function generator with a load resistor of 0-300 Ω. A diagram of the resistor setup was presented in the Supplementary Material of Ref [9]. The current and voltage applied to the mesa were monitored by two different commercial digital multimeters. The liquid Helium cooled Si-bolometer was used for the detection of THz radiation. The frequency was measured using the Fourier transform infrared spectrometer (JASCO FARIS-1).

Table 1. Sample bottom shape and T_c parameters

Sample No.	Mesa Shape	*b* (μm)	*a* (μm)	Thickness (μm)	T_c (ΔT_c) K
1	Equilateral	102.5	102.5	1.2	78.5 (2.2)
2	Equilateral	85	85	1.2	75.9 (3.4)
3	Equilateral	90	90	1.3	75.6 (0.3)
4	Isosceles	90	340	1.3	79.8 (1.8)
5	Isosceles	90	320	1.2	74.8 (1.3)

3. Experimental results and discussion

3.1 Equilateral triangular mesas

In order to summarize how the experiments are performed and also to emphasize the differences between highly tunable radiation and the radiation that involves strong locking of the frequency $f = f_J$ onto a cavity mode frequency f^c_{mn}, we begin with the first emission data obtained from an equilateral triangular Bi-2212 mesa. The temperature dependence of the *c*-axis resistance *R (T)* of an equilateral triangular mesa (sample 3) is presented in Fig. 2(a). The room temperature resistance (R_{RT}) of the mesa is 28.5 Ω while the resistance at around T_c (R_{TC}) is 98.5 Ω. The residual resistance of this sample is 11 Ω, which was subtracted from *R (T)*, as for all samples investigated in this study.

#179100 - $15.00 USD Received 5 Nov 2012; revised 28 Dec 2012; accepted 29 Dec 2012; published 22 Jan 2013

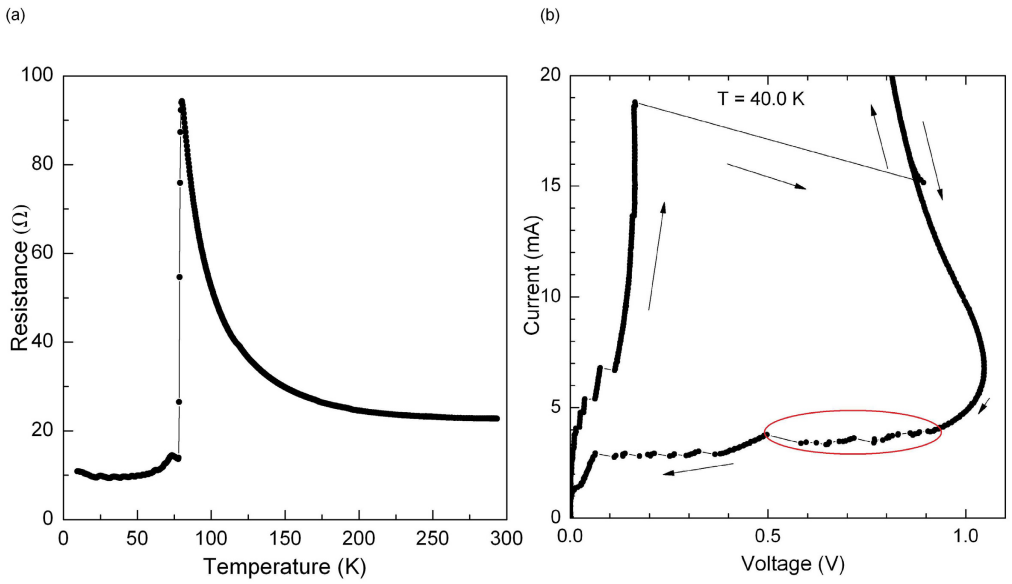

Fig. 2. (a) The temperature dependence of the *c*-axis resistance of sample 3. (b) Outer branch IVCs for sample 3 at the bath temperature $T = 40.0$ K. The arrows indicate the cycle direction. The red ellipse identifies the region of irreversible IVC jumps.

In Fig. 2(b), we show a typical example of the outermost branch of the IVCs obtained from sample 3 at $T = 40.0$ K. The IVCs exhibit negative differential resistance and sharp drops in V near the retrapping current $I = 3$ mA, as shown in Fig. 2(b). This back-bending feature of the *I*-*V* curve indicates a considerable Joule heating of several mW in Bi-2212 samples [13,14]. The emission signal detected by the Si-bolometer is shown in Fig. 3(a). For this sample, we observed emissions around the retrapping region where $I = 4$~5 mA and $V = 0.5$~0.94 V. These emissions are observed in a bath temperature range between $T = 30.0$ and 55.0 K. In the retrapping region, the IVCs show small jumps which indicate the change in the number of resistive junctions, and the IVCs and the emission are irreversible when sweeping the current. Thus, the emission observed in this region (denoted by the red ellipse) is classified as an irreversible (IR) type emission [16]. The corresponding spectra measured using the Fourier transform infrared spectrometer at $V = 0.91$ V in the IVCs in Fig. 2(b) is shown in Fig. 3(b).

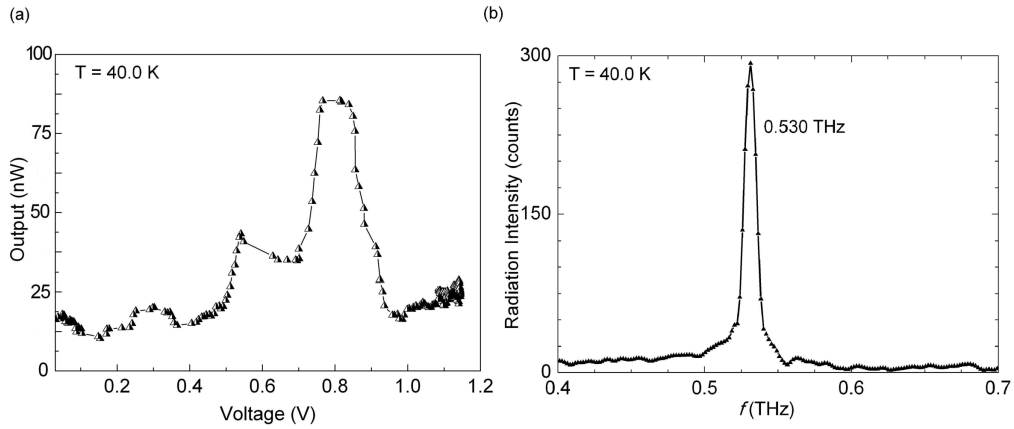

Fig. 3. (a) The emission signal from sample 3 detected by the Si-bolometer. (b) The measured spectra using the Fourier transform infrared spectrometer at 0.91 V.

#179100 - $15.00 USD Received 5 Nov 2012; revised 28 Dec 2012; accepted 29 Dec 2012; published 22 Jan 2013

The measured frequency of the emission is 0.530 THz. According to the ac-Josephson relation $f = f_J = (2e/h)V/N$, in this example, N = 830 junctions were involved in the radiation. The cavity modes in an equilateral triangular resonator are expressed using two indices m and n, and the transverse magnetic cavity resonant frequencies are given by $f_{mn}^{c} = (2c_0 / 3an_r)(m^2 + mn + n^2)^{1/2}$ [25–27], where c_0 is the velocity of light in free space, a is the length of a side of the triangle, n_r is the dielectric constant of the substrate, and m, n are natural numbers. If we take n_r = 4.2 as in all other samples [8,29], the emission frequency of 0.530 THz observed from sample 3 almost satisfies the cavity resonance frequency of 0.529 THz from the highly degenerate $\mathrm{TM}(0,1) = \mathrm{TM}(1,0) = \mathrm{TM}(1,-1)$ modes. We have determined that each of these modes actually consists of six degenerate TM modes. There are three even and three odd wave functions about a line drawn from a corner to the midpoint of an opposite side [30]. This mode degeneracy is much higher than in all of the rectangular, disk, and nearly square mesas studied to date, and is likely responsible for the limitation of the emission frequencies to the single $f = f_J = f_{10}^{c}$ mode frequency we observed.

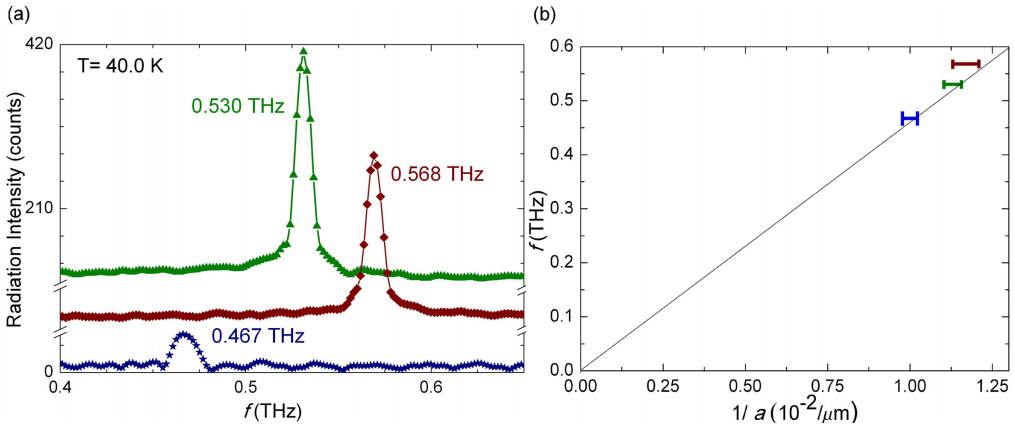

Fig. 4. (a) The emission spectra measured by the Fourier transform infrared spectrometer for three equilateral triangular mesas. The blue, red, and green curves correspond to samples 1, 2, and 3, respectively. (b) The measured frequencies as a function of 1/a. The error bars indicate the trapezoidal mesa cross sections and the peak widths at half maximum in Fig. 4(a). The line corresponds to the fundamental $\mathrm{TM}(0,1) = \mathrm{TM}(1,0) = \mathrm{TM}(1,-1)$ cavity resonance frequency.

Figure 4(a) shows the emission at the frequencies 0.467, 0.568 and 0.530 THz measured by the Fourier transform infrared spectrometer at 40.0 K for three equilateral triangular mesas (samples 1, 2, and 3, respectively) whose side lengths a are different from one another. In Fig. 4(b), the emission frequencies of these samples are plotted as a function of 1/a. The line indicates the frequency of the fundamental equilateral triangular mode frequency f_{10}^{c} with n_r = 4.2. This figure shows that the resonant frequency is inversely proportional to the side length of the equilateral triangular mesas, and well satisfies the cavity resonance relation $f = f_{10}^{c}$. From the Si-bolometer measurement of 8 mV, taking account of the window in our cryostat and our angular output power measurements not shown here, we estimate the integrated output power as ~0.1 μW [9].

3.2 Isosceles triangular mesas

Dramatically different behavior was observed from isosceles triangular mesas. The return branch of the IVCs for sample 4 is shown in Fig. 5(a) and its emission intensity as detected by the Si-bolometer is shown as a function of current in Fig. 5(b).

#179100 - $15.00 USD Received 5 Nov 2012; revised 28 Dec 2012; accepted 29 Dec 2012; published 22 Jan 2013

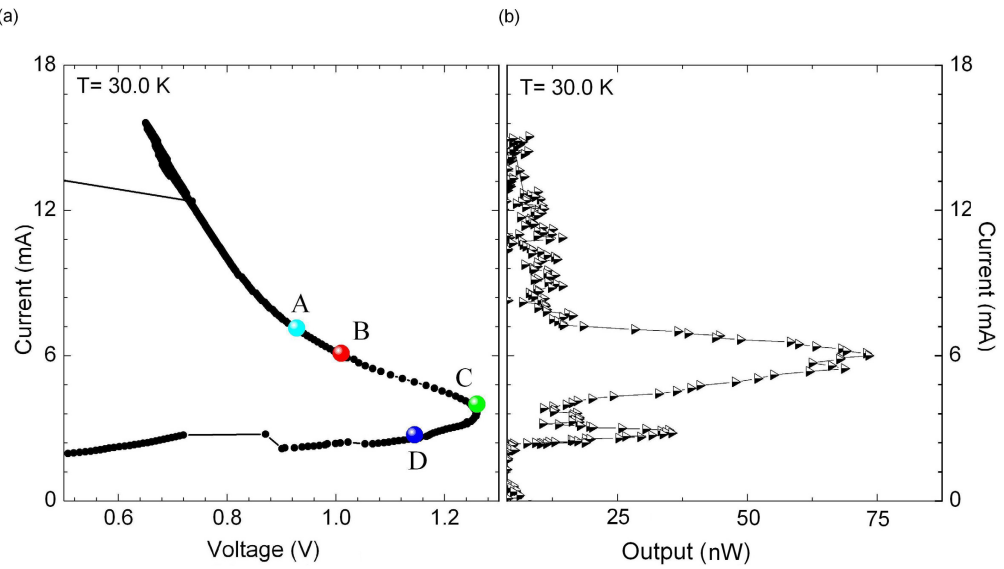

Fig. 5. (a) The only return branch of the outer-branch *I-V* curve obtained from an acute isosceles triangular mesa (sample 4) measured at bath temperature T = 30.0 K. (b) The emission intensity from sample 4 detected by the Si-bolometer is plotted as a function of I.

As seen in Fig. 5(a), the *I-V* curve bends backward with increasing current similar to the *I-V* curve in Fig. 2(b). For this sample, THz waves were observed in the high voltage region where the IVCs show negative differential resistance. Emission was observed over the wide current range of 2 to 7 mA, with broad emission peaks occurring from 3 to 7 mA. Since the IVCs are reversible, the emission observed in this region is classified as reversible (R) type emission [16]. Figure 6(a) shows the measured frequency spectra obtained from the Fourier transform infrared spectrometer corresponding to the four points A to D indicated by the color symbols in Fig. 5(a). The measured frequencies are plotted as a function of bias voltage in Fig. 6(b). The straight line shows the expected $f = f_J$ from the ac-Josephson relation with the number of working junctions $N_{\text{fit}} = 720$ obtained from $N_{\text{fit}} = (2eV/hf)$.

Figure 6(b) shows that the observed frequencies well satisfy the ac-Josephson relation with a fixed value N_{fit} of active IJJs [9,16]. However, in previous reports using different samples [14,17,21], it was found that only 83% of the IJJs were active. In the present case, our only uncertainty is the direct measurement of the sample 4 thickness of 1.3 μm is due to the unknown top Ag and Au layer thicknesses, which we could estimate as about 10 nm. Neglecting this uncertainty would lead to 850 junctions in the sample, which would lead to about 85% of the IJJs being active, in agreement with those previous reports [14,17,21].

#179100 - $15.00 USD Received 5 Nov 2012; revised 28 Dec 2012; accepted 29 Dec 2012; published 22 Jan 2013

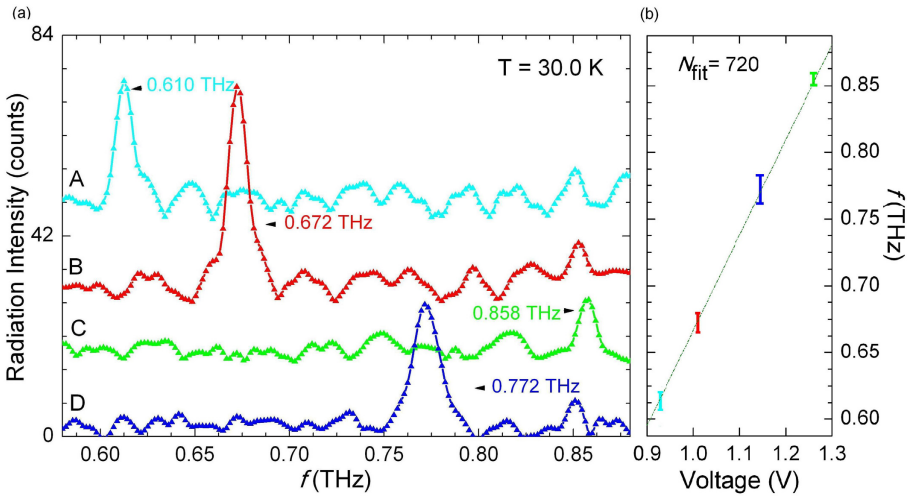

Fig. 6. (a) Radiation spectra from sample 4 measured by the Fourier transform infrared spectrometer at the *I-V* points A-D corresponding to the symbols in Fig. 5(a). (b) The measured frequencies are plotted as a function of the bias voltage. The error bars are the peak widths at half maximum. The straight line passing through the origin is a fit to the ac-Josephson relation with $N_{fit} = 720$ active junctions.

We also plotted the measured frequency as a function of the bath temperature T for sample 4 as shown in Fig. 7(a). For this sample, we observed THz emission in the temperature range between $T = 10.0$ and 50.0 K. With increasing T, the emission region on the *I-V* curve shifts to lower current bias, and the values and the ranges of the emission frequencies both decrease. By changing both V and T, we could tune the emission frequency from 0.495 to 0.934 THz. This frequency tunability of 47% obtained from the outermost IVC branch is larger than those reported in previous studies of rectangular mesa samples [9,14,22]. It is noteworthy that for T varying in increments of 5.0 K from 10.0 to 50.0 K, the observed emission frequency varies from 0.495 to 0.934 THz. Wang *et al.* [14] also reported a strong T dependence to the emission frequency range. However our results obtained from sample 4, show that with increasing T, the range of emission frequencies is the smallest at $T = 10.0$ K, increases to a maximum at $T = 25.0$ K, and then gradually decreases until it vanishes above $T = 50.0$ K, at which the minimum emission frequency reaches its overall lowest value of 0.495 THz.

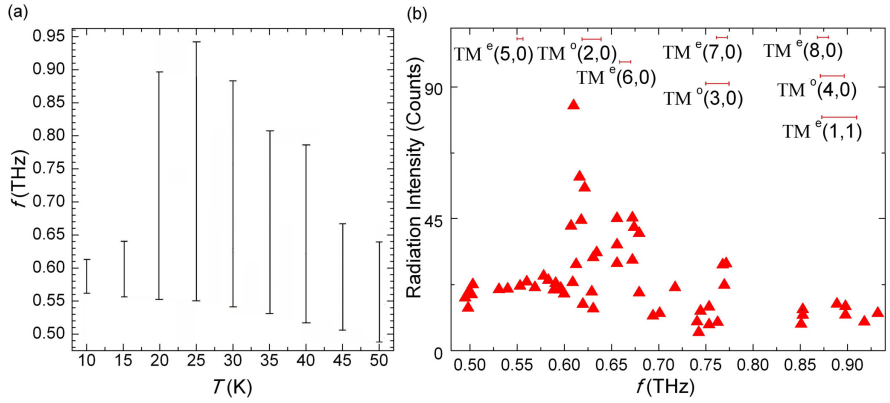

Fig. 7. (a) The bath temperature dependence of the measured emission frequencies from the outermost *I-V* branch of sample 4. (b) The overall emission intensity for T varying from 10.0 to 50.0 K in increments of 5.0 K as a function of frequency for this sample. The ranges due to the trapezoidal sample cross section of the wedge cavity mode frequencies calculated in section 4.2 are listed at the figure top.

#179100 - $15.00 USD Received 5 Nov 2012; revised 28 Dec 2012; accepted 29 Dec 2012; published 22 Jan 2013

Although Fig. 6(b) provides strong evidence that the ac-Josephson current is the primary radiation source in sample 4 [9,11,18–20,31], the wide range of radiation frequencies exhibited in Fig. 7 suggests that the cavity resonance mechanism might be at best of secondary importance. Figure 7(b) shows that the overall frequency spectrum of the emission intensity is essentially continuous, as the apparent small gaps between points at which the emission was observed could merely reflect details of the experimental technique. However, Fig. 7(b) clearly indicates that the strongest emission is observed just above 0.6 THz. This feature strongly suggests that one or more resonance modes might appear around and somewhat above this frequency. Nevertheless, by comparing ranges of the expected wedge cavity resonances presented at the top of Fig. 7(b), it is clear that there exist wide *f* ranges for which radiation occurs, but no cavity resonances are predicted. This wide 47% tunability from 0.495 to 0.934 THz strongly suggests that acute triangular mesa shapes can greatly aid in the development of a useful device.

We measured the angular dependence of the radiation in two orthogonal planes for both samples 3 and 4, but the results will be presented elsewhere, along with detailed fits to the data, as was done previously for rectangular and cylindrical mesas [9,11,20]. From these angular distributions and the measurement of the output voltage of up to 7 mV in our Si-bolometer for the maximum at 0.61 THz, we estimate the integrated output power as ~0.1 μW [9]. These values are somewhat lower than has been reported previously, but in the case of the isosceles triangular mesas, the tunability of the mesas allows the experimenter to enhance the overall output by placing the mesa in a tunable external EM cavity that can be independently controlled, thereby increasing the overall output power significantly [9].

4. Theoretical studies of isosceles triangles

4.1 Numerical studies of sample 4

Since an analytical solution for the TM cavity modes in a general isosceles triangular resonator has not yet been published, we investigated the TM modes of an EM cavity of such isosceles triangular shapes using both a numerical and an analytical technique. First, we numerically investigated the EM modes in a thin isosceles triangular mesa with the geometry of sample 4. We assumed the motion of each of the superconducting phase differences across the IJJs within the mesa are perfectly synchronized, and then simultaneously calculated the EM fields inside and outside of the IJJs [32].

In Fig. 8, we show a sketch representing the geometry of sample 4 and the numerical model we studied. In this calculation, we assumed the appearance of a “hot spot” induced by local heating around the region where the current lead is attached to the Bi-2212 mesa. We model the heating effects by the creation of an inhomogeneous critical current, setting the critical current of this red-and-white striped rectangular hot spot region to be 75% of that of rest of the sample. Such inhomogeneities were considered to be important for the excitation of a transverse plasma wave within IJJs [32,33], and were inferred from experimental studies [14]. In previous studies, we found that removing or changing the location of the hot spot can lead to changes in the cavity mode excitations [32]. The parameters used in the numerical calculation are as follows: the *c*-axis conductivity is taken to be 5 S, λ_c, the *c*-axis penetration depth is assumed to be 250 μm, the dielectric constant within each junction is 17.64, and the thicknesses of the superconducting and insulating layers are 0.3 nm and 1.2 nm, respectively. The value of λ_c is comparable to that of Bi-2212 measured at low and intermediate temperatures, as its temperature dependence below 50 K is very weak [34,35].

#179100 - $15.00 USD Received 5 Nov 2012; revised 28 Dec 2012; accepted 29 Dec 2012; published 22 Jan 2013

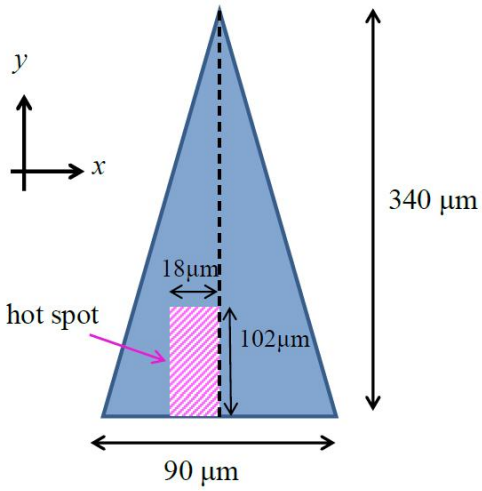

Fig. 8. Sketch of the numerical calculation model for sample 4, including the hot spot and the sample dimensions.

Figure 9(a) shows the calculated emission power spectrum obtained from our numerical model. In this figure, a sharp resonance-like peak appears around 0.61 THz. This frequency is almost equal to the peak frequency observed in the experiments on sample 4. In Fig. 9(b), we show the amplitude map of the electric field, E_z, at this frequency. In this figure, a standing wave mode that is antisymmetric both across the bisector of the acute angle and across a line parallel to the base of the isosceles triangular mesa is clearly evident [36]. This is in agreement with our analytic calculation of the $TM^{o}(2,0)$ mode presented in Section 4.2. From previous calculations and experiments, such antisymmetric modes usually lead to substantial radiation directly atop the mesa [17–20].

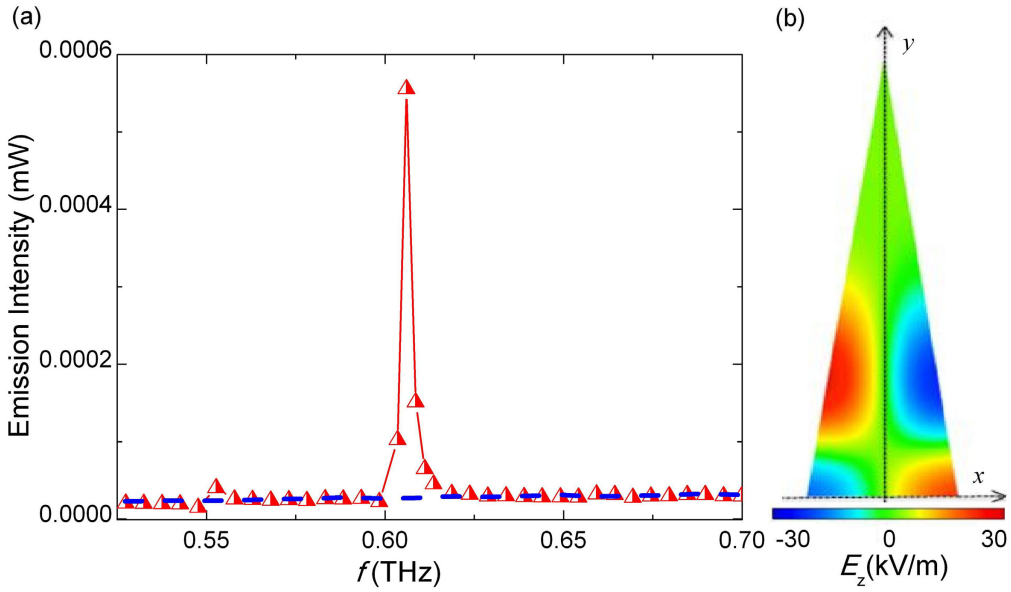

Fig. 9. (a) The emission power frequency spectrum calculated with the hot spot (Red) and without it (blue) from our numerical model of sample 4. (b) The amplitude map of the electric field, E_z, at 0.61 THz calculated using our numerical model of sample 4. An anti-symmetric standing-wave resonant mode very similar to the $TM^{o}(2,0)$ wedge mode is shown.

#179100 - $15.00 USD Received 5 Nov 2012; revised 28 Dec 2012; accepted 29 Dec 2012; published 22 Jan 2013

4.2 Approximate analytic solution of highly acute isosceles triangular patch antennas

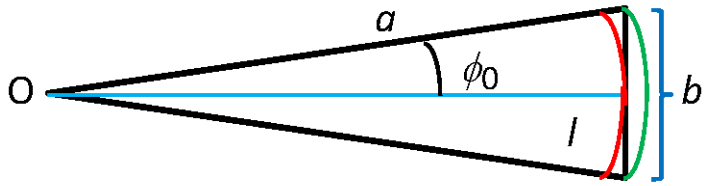

Fig. 10. Pie-shaped wedge approximation to the shape of a thin acute isosceles triangular patch antenna. The red and green curves are circular arcs of radii a and l = $[a^2 - (b/2)^2]^{1/2}$, respectively.

Since no analytic solution of the TM modes in a general thin isosceles triangular patch antenna has been published, we studied two exactly soluble models, which both become exact in the limit of an infinitely acute isosceles triangle. Both models are extremely simple: we approximate the acute triangle as one of two thin pie-shaped wedges, which are sketched in Fig. 10. In both models, the acute angle is taken to be $2\phi_0 = 2\sin^{-1}(b/2a)$, where a and b are the long and short sides of the isosceles triangle, respectively. In model 1, the short side b of the isosceles triangle is approximated as a circular arc of radius a, and in model 2, it is approximated as a circular arc of radius $l = [a^2 - (b/2)^2]^{1/2}$. Thus, in model 1, the sides of the isosceles triangle are equal to a, the actual side lengths, and in model 2, the arc is tangent to the short side. Thus, the shape of the acute isosceles triangle is intermediate between that of models 1 and 2.

These models are easily solved by separation of variables in polar coordinates (ρ,ϕ). For either model 1 or model 2, the magnetic vector potential A_z can be either even or odd about the horizontal line $\phi = 0$. To satisfy the TM boundary conditions, one simply takes the derivative of A_z normal to each of the three edges of each wedge to vanish. From $\partial A_z / \partial\phi\big|_{\phi=\pm\phi_0} = 0$, we obtain $A_z^e(\rho,\phi) = C^e \cos(\nu_n^e \phi) J_{\nu_n^e}(k\rho)$, $\nu_n^e = n\pi/\phi_0$, $n = 0,1,2,...$ for the even modes and $A_z^o(\rho,\phi) = C^o \sin(\nu_n^o \phi) J_{\nu_n^o}(k\rho)$, $\nu_n^o = (n+1/2)\pi/\phi_0$, $n = 0,1,2,...$ for the odd modes, where they $C^{(o,e)}$ are constants. From the remaining TM boundary condition, $\partial A_z / \partial\rho\big|_{\rho=a,l} = 0$ for models 1 and 2, respectively, the eigenvalues are simply given by $J'_{\nu_n^{(o,e)}}(k_m a) = 0$ in model 1 and $J'_{\nu_n^{(o,e)}}(k_m l) = 0$ in model 2, where $J'_\nu(x)$ is the first derivative of the Bessel function $J_\nu(x)$ of the first kind. For highly acute isosceles triangles such as that of sample 4, a = 340 μm and l = 337 μm differ by less than 1%, so these solutions are sufficiently accurate for precise comparison with experiment. The mode frequencies are then given by $f_{mn}^{(o,e)} = c_0 \chi(m, \nu_n^{(o,e)}) / [2n_r \pi (a,l)]$, where $\chi(m, \nu_n^{(o,e)})$ is the mth zero of the first derivative of $J_{\nu_n^{(o,e)}}(x)$, and the denominator is either $2n_r\pi a$ for model 1 or $2n_r\pi l$ for model 2.

Table 2 presents the lowest eigenvalues $\chi(m, \nu_n^{(o,e)})$ and the corresponding mode frequencies $f_{mn}^{(o,e)}$ for model 1 with the shape parameters of sample 4. For this mesa, $\nu_0^e = 0$, $\nu_0^o = 11.8331$, and $\nu_1^e = 23.6662$. We note that this table shows that the odd cavity resonances appear to play a significant role in understanding the observed emission intensity spectrum of sample 4 shown in Fig. 7(b). In particular, the first odd cavity resonance is expected to be at 0.462 THz, just below the minimum value of the observed emission frequencies. The second odd cavity resonance is almost exactly in agreement with the frequency (0.624 THz) of the narrow maximum in the emission intensity spectrum, and the

#179100 - $15.00 USD Received 5 Nov 2012; revised 28 Dec 2012; accepted 29 Dec 2012; published 22 Jan 2013

third odd frequency at 0.754 THz is in general agreement with the region in the observed frequency spectrum of the second largest emission. In addition, some of the even modes could enhance this spectrum, giving five possible resonances from 0.550 THz to 0.876 THz. Thus, this exact solution to the approximate model(s) of acute isosceles triangular mesas can give a very accurate accounting of the peaks in the observed intensity spectrum of sample 4.

Table 2. The lowest eigenvalues $\chi(m,\nu_n^{(o,e)})$ and model 1 frequencies $f_{mn}^{(o,e)} = c_0\chi(m,\nu_n^{(o,e)})/[2n_r\pi(a,l)]$ for sample 4.

m	$\chi(m,\nu_0^e)$	f(THz)	$\chi(m,\nu_0^o)$	f(THz)	$\chi(m,\nu_1^e)$	f(THz)
1	3.8317	0.128	13.70	0.458	26.01	0.869
2	7.0156	0.234	18.55	0.620	31.74	1.06
3	10.1735	0.340	22.43	0.749	36.16	
4	13.3237	0.445	26.04	0.870	40.17	
5	16.4706	0.550	29.52	0.986		
6	19.6158	0.655	32.92	1.10		
7	22.7601	0.760				
8	25.9037	0.866				
9	32.1897	1.076				

In Fig. 7(b), we included the ranges of the expected wedge cavity frequencies due to the trapezoidal cross section of the mesa. The peaks in the spectrum at 0.61 and 0.65-0.68 THz appear to be close to the wedge TM_{20}^o and TM_{60}^e modes, respectively. We note that the largest resonance is for a wave function of odd symmetry about the line $\phi = 0$, which is in agreement with the numerical pattern shown in Fig. 9(b). This odd symmetry seems to correlate well with most results for rectangular and cylindrical mesas [7–21]. However, in general, most of the observed spectrum does not correlate well with the predicted wedge cavity resonances, providing support to the notion that the primary mechanism for the radiation is the ac-Josephson current source itself.

In order to calculate the expected radiation pattern from each of these modes and from the uniform ac-Josephson current source, one needs to use the Love equivalence principles to obtain the effective surface electric and magnetic currents [11,18,19]. This will be calculated, and fits to the angular dependence of the radiation observed from samples 3 and 4 be given in a subsequent publication.

5. Conclusions

For further understanding of the role of the internal cavity for THz radiation from IJJs mesas, triangular mesa shapes were studied both experimentally and theoretically. Continuous and coherent THz EM waves were observed from the intrinsic Josephson junctions present in both equilateral and acute isosceles triangular mesas of single crystalline high temperature superconducting $Bi_2Sr_2CaCu_2O_{8+\delta}$. We studied experimentally the *I-V* characteristics and the emission spectra using the Fourier transform infrared spectrometer in order to elucidate the radiation mechanism of the triangular mesa samples. For equilateral triangular mesas, THz radiation was only observed when the emission frequency was in the vicinity of the lowest cavity resonant frequency determined by the mesa geometry. However, in strong contrast, for an isosceles triangular mesa, THz radiation was observed over the wide frequency range of 0.495 to 0.934 THz, and the frequency dependence of the emission power exhibited an overall sharp peak. This frequency tunability of 47% from the outermost branch of the *I-V* curve is the largest observed to date, regardless of the sample geometry. We numerically investigated the internal EM cavity modes of the IJJ mesas using the finite difference time domain method, and modeled the acute isosceles triangular mesa as a pie-shaped wedge. In both calculations, the peak frequency of the emission agrees well with a cavity resonance frequency of the isosceles triangular mesa. However, most of the radiation observed in

#179100 - $15.00 USD Received 5 Nov 2012; revised 28 Dec 2012; accepted 29 Dec 2012; published 22 Jan 2013

experiment was at frequencies that could not be ascribed to any particular cavity resonance. Therefore, the most important feature of this work is the observation that acute isosceles triangular mesas offer the best method to date for optimizing the radiation tunability.

Acknowledgments

This work has been supported in part by CREST-JST (Japan Science and Technology Agency), and WPI (World Premier International Research Center Initiative)-MANA (Materials Nanoarchitectonics) project (NIMS).

#179100 - $15.00 USD Received 5 Nov 2012; revised 28 Dec 2012; accepted 29 Dec 2012; published 22 Jan 2013